

# Searching for spiral features in the outer Galactic disk.

## The field towards WR38 and WR38a

Giovanni Carraro<sup>1,2</sup> and Edgardo Costa<sup>3</sup>

<sup>1</sup>ESO, Casilla 19001, Santiago, Chile

<sup>2</sup>Dipartimento di Astronomia, Università di Padova, Vicolo Osservatorio 2, I-35122 Padova, Italy

<sup>3</sup>Departamento de Astronomía, Universidad de Chile, Casilla 36-D, Santiago, Chile

Received ....; accepted...

### ABSTRACT

**Context.** The detailed spiral structure in the outer Galactic disk is still poorly known, and for several Galactic directions we still have to rely on model extrapolations.

**Aims.** One of these regions is the fourth Galactic quadrant, in the sector comprised between Vela and Carina ( $270^\circ \leq l \leq 300^\circ$ ) where -apart from the conspicuous Carina branch of the Carina Sagittarius arm- no spiral arms have been detected so far in the optical beyond  $l \sim 270^\circ$ .

**Methods.** By means of deep *UBVI* photometry, we search for spiral features in known low absorption windows. *U* photometry, although observationally demanding, constitutes a powerful tool to detect and characterize distant aggregates of young stars, and allows to derive firmer distance estimates. We have studied a direction close to the tangent ( $l \sim 290^\circ$ ) to the Carina arm, in an attempt to detect optical spiral tracers far beyond the Carina branch, where radio observations and models predictions seem to indicate the presence of the extension of the Perseus and Norma-Cygnus spiral arms in the fourth quadrant.

**Results.** Along this line of sight, we detect three distinct groups of young stars. Two of them, at distances of  $\sim 2.5$  and  $\sim 6.0$  kpc, belong to the Carina spiral arm (which is crossed twice in this particular direction). Interestingly, the latter is here detected for the first time. The third group, at a distance of  $\sim 12.7$  kpc, is likely a part of the Perseus arm which lies beyond the Carina arm, and constitutes the first optical detection of this arm in the fourth Galactic quadrant. The position of this feature is compatible both with HI observations and model predictions. We furthermore present evidence that this extremely distant group, formerly thought to be a star cluster (Shorlin 1), is in fact a diffuse young population typical of spiral features. In addition, our data-set does not support, as claimed in the literature, the possible presence of the Monoceros Ring toward this direction

**Conclusions.** This study highlights how multicolor optical studies can be effective to probe the spiral structure in the outer Galactic disk. More fields need to be studied in this region of the Galaxy to better constrain the spiral structure in the fourth Galactic quadrant, in particular the shape and extent of the Perseus arm, and, possibly, to detect the even more distant Norma-Cygnus arm.

**Key words.** Galaxy: spiral arms- Open clusters and associations: general- Open clusters and associations: individual: Shorlin 1

## 1. Introduction

In recent times the study of the spiral structure of the outer Galactic disk has witnessed a renewed interest (see e.g. Levine et al. 2006, Vázquez et al. 2008, Benjamin 2008), in part due to the claimed discovery of structures in the form of star over-densities which would be produced by accretion/merging events. Examples are those in Monoceros (Yanny et al. 2003), Canis Major (Martin et al. 2004) and Argus (Rocha Pinto et al. 2006). To assess the reality and properties of these over-densities, a detailed investigation of the outer Galactic disk is a basic requirement. Such an investigation would also improve our knowledge of the extreme periphery of the Milky Way (MW).

Spiral features can be detected by using a variety of tracers, namely HI (see e.g. Levine et al. 2006), HII (see e.g. Russeil 2003), CO (see e.g. Luna et al. 2006), and optical objects (see e.g. Vázquez et al. 2008). These diverse techniques have provided a coherent picture of the spiral structure in the third

Galactic quadrant (Moitinho et al. 2008). Our group has contributed to this effort providing optical information for a large sample of young open clusters (Moitinho et al. 2006), in the field of which we have recognized distant and reddened sequences which allowed us to define the shape and extent of spiral arms up to 20 kpc from the Galactic center.

This paper is the first result of a study of selected low-absorption regions in the fourth Galactic quadrant, aimed at finding distant optical spiral features. We present an investigation of the field towards the Wolf-Rayet (WR) stars WR38 and WR38a ( $RA = 11^h06^m$ ,  $DEC = -61^\circ14'$ , Shorlin et al. 2004, hereafter Sh04; Wallace et al. 2005, hereafter Wa05), which attracted our attention for several reasons.

Sh04 and Wa05 discuss the discovery of a distant, young, compact star cluster, at a distance of  $\sim 12$  kpc, associated with these two WR stars. These two studies, however, reach quite different conclusions about the relationship of this cluster with known spiral arms. While Sh04 propose that the cluster is associated with an extension of the Perseus arm beyond the Carina-Sagittarius arm, Wa05, more conservatively, suggest that

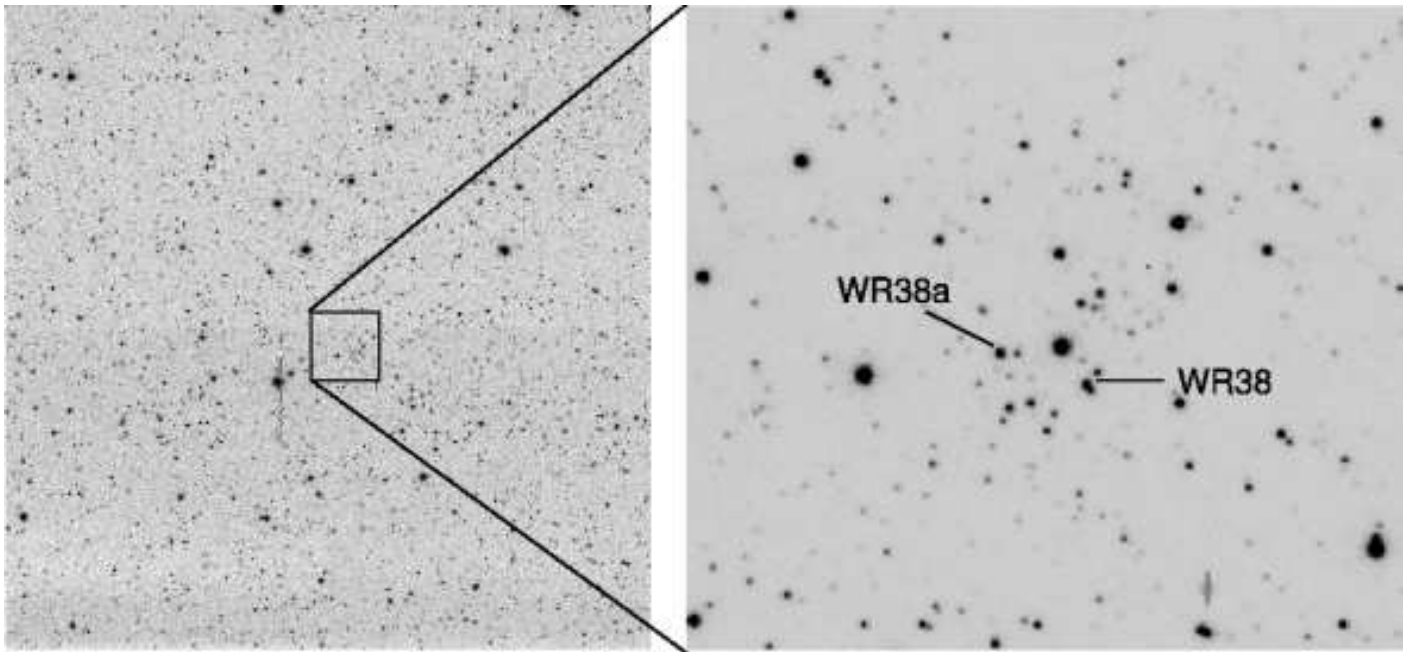


**Fig. 1.** Left panel: *V*-band 100 sec exposure image of the field observed in the area of the star cluster Shorlin 1. Field shown is 20' on a side. North is up and East to the left. Right panel: Zoom of the cluster region, in which the two WR stars (WR38 and WR38a) are indicated. Field shown is  $\sim 3'$  on a side.

it lies in the more distant part of the Carina arm. In fact, the line-of-sight in the direction to WR38 and WR38a crosses twice the Carina-Sagittarius arm. In a quite different interpretation, Frinchaboy et al. (2004) associate this cluster to the Galactic Anticenter Stellar Structure (GASS), a population of old star clusters, possibly members of the Monoceros Ring.

With the purpose of clarifying these issues, we undertook an observational campaign which addresses the following questions: Is the group of stars close to WR38 and WR38a (i.e. Shorlin 1) a real star cluster? Does this group belong to the most distant part of the Carina arm or to the Perseus arm? Are we looking in this direction at signatures of the Monoceros ring, or the Argus system?

The paper is organized as follows. In Sect 2 we describe the observations and the reduction procedure and compare our dataset with previous investigations, and in Sect. 3 we discuss the reddening law in the Galactic direction under consideration. In Sect. 4 and 5 we thoroughly discuss the properties of the three different stellar populations detected in the field observed. Finally, Sec. 6 summarizes the results of our study.

## 2. Observations and Data Reduction

### 2.1. Observations

The region of interest (see Fig. 1) was observed with the Y4KCAM camera attached to the 1.0m telescope, which is operated by the SMARTS consortium<sup>1</sup> and located at Cerro Tololo Inter-American Observatory (CTIO). This camera is equipped with an STA 4064 $\times$ 4064 CCD with 15- $\mu$  pixels, yielding a scale of 0.289"/pixel and a field-of-view (FOV) of 20'  $\times$  20' at the Cassegrain focus of the CTIO 1.0m telescope. The CCD was operated without binning, at a nominal

**Table 1.** Log of *UBVI* photometric observations.

Target	Date	Filter	Exposure (sec)	airmass
Shorlin 1	24 May 2006	U	60, 1500	1.28–1.33
		B	30, 100, 1200	1.20–1.35
		V	30, 100, 900	1.22–1.34
		I	100, 700	1.25–1.34
Shorlin 1	29 January 2008	U	5, 15	1.19–1.22
		B	3, 5, 10	1.19–1.23
		V	3, 5, 10	1.18–1.22
		I	3, 5, 10	1.18–1.23
SA 98	29 January 2008	U	2x10, 200, 300, 400	1.17–1.89
		B	2x10, 100, 2x200	1.17–1.99
		V	2x10, 25, 50, 2x100	1.20–2.27
		I	2x10, 50, 100, 2x150	1.18–2.05
Shorlin 1	05 June 2008	U	30x3, 1800	1.19–1.20

gain of 1.44 e<sup>-</sup>/ADU, implying a readout noise of 7 e<sup>-</sup> per quadrant (this detector is read by means of four different amplifiers). QE and other detector characteristics can be found at: <http://www.astronomy.ohio-state.edu/Y4KCam/detector.html>.

The observational material was obtained in three observing runs, resumed in Table 1. In our first run we took deep *UBVI* images of Shorlin 1, under good seeing, but non-photometric conditions. In our second run we took medium and short exposures of Shorlin 1, and observed Landolt's SA 98 *UBVRI* standard stars area (Landolt 1992), to tie our *UBVI* instrumental system to the standard system. In a final third run we secured an additional set of *U*-band images of Shorlin 1. Average seeing was 1.2".

Our *UBVI* instrumental photometric system was defined by the use of a standard broad-band Kitt Peak *BVR<sub>kc</sub>I<sub>kc</sub>* set in combination with a U+CuSO<sub>4</sub> *U*-band filter. Transmission curves for these filters can be found at:

<sup>1</sup> <http://http://www.astro.yale.edu/smarts>

<http://www.astronomy.ohio-state.edu/Y4KCam/filters.html>. To determine the transformation from our instrumental system to the standard Johnson-Kron-Cousins system, we observed 46 stars in area SA 98 (Landolt 1992) multiple times, and with different airmasses ranging from  $\sim 1.2$  to  $\sim 2.3$ . Field SA 98 is very advantageous, as it includes a large number of well observed standard stars, and it is completely covered by the CCD's FOV. Furthermore, the standard's color coverage is very good, being:  $-0.5 \leq (U - B) \leq 2.2$ ;  $-0.2 \leq (B - V) \leq 2.2$  and  $-0.1 \leq (V - I) \leq 6.0$ .

## 2.2. Reductions

Basic calibration of the CCD frames was done using the IRAF<sup>2</sup> package CCDRED. For this purpose, zero-exposure frames and twilight sky flats were taken every night. Photometry was then performed using the IRAF DAOPHOT and PHOTCAL packages. Instrumental magnitudes were extracted following the point spread function (PSF) method (Stetson 1987). A quadratic, spatially variable, Master PSF (PENNY function) was adopted. The PSF photometry was finally aperture-corrected, filter by filter. Aperture corrections were determined performing aperture photometry of a suitable number (typically 10 to 20) of bright stars in the field. These corrections were found to vary from 0.120 to 0.215 mag, depending on the filter.

## 2.3. The photometry

Our final photometric catalog consists of 7425 entries having *UBVI* measures down to  $V \sim 20$ , and 12250 entries having *BVI* measures down to  $V \sim 22$ .

After removing saturated stars, and stars having only a few measurements in Landolt's (1992) catalog, our photometric solution for a grand-total of 183 measurements in *U* and *B*, and of 206 measurements in *V* and *I*, turned out to be:

$$\begin{aligned} U &= u + (3.290 \pm 0.010) + (0.47 \pm 0.01) \times X - (0.010 \pm 0.016) \times (U - B) \\ B &= b + (2.220 \pm 0.012) + (0.29 \pm 0.01) \times X - (0.131 \pm 0.012) \times (B - V) \\ V &= v + (1.990 \pm 0.007) + (0.16 \pm 0.01) \times X + (0.021 \pm 0.007) \times (B - V) \\ I &= i + (2.783 \pm 0.011) + (0.08 \pm 0.01) \times X + (0.043 \pm 0.008) \times (V - I) \end{aligned}$$

The final *r.m.s.* of the fitting was 0.073, 0.069, 0.035 and 0.030 in *U*, *B*, *V* and *I*, respectively.

Global photometric errors were estimated using the scheme developed by Patat & Carraro (2001, Appendix A1), which takes into account the errors resulting from the PSF fitting procedure (e.i. from ALLSTAR), and the calibration errors (corresponding to the zero point, color terms and extinction errors). In Fig. 2 we present global photometric error trends plotted as a function of *V* magnitude. Quick inspection shows that stars brighter than  $V \approx 20$  mag have errors lower than 0.10 mag in magnitude and lower than 0.20 mag in all colors.

The only previous *UBV* (Johnson-Morgan) photometric study of this region is that of Sh04, who present photoelectric

<sup>2</sup> IRAF is distributed by the National Optical Astronomy Observatory, which is operated by the Association of Universities for Research in Astronomy, Inc., under cooperative agreement with the National Science Foundation.

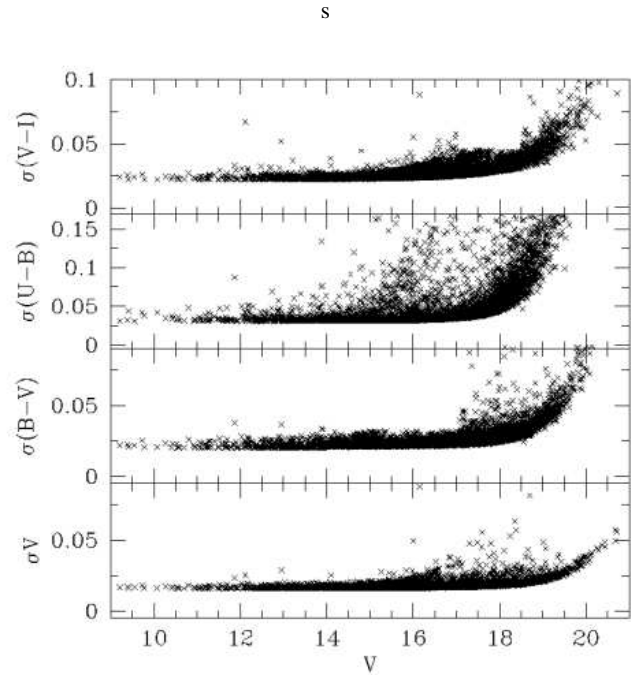


**Fig. 2.** Photometric errors in *V*, (*B-V*), (*U-B*) and (*V-I*) as a function of *V* mag.

and CCD photometry for roughly 140 stars brighter than  $V \sim 16.5$  in the field of WR38 and WR38a. In Fig. 3, we compare our photometry with that of Sh04 for *V*, *B - V* and *U - B*, in the sense ours minus theirs, as a function of our *V* magnitude. This comparison was possible only for 103 of their stars because, from the material presented in Sh04, it was not possible to identify all objects measured by them (this issue was addressed with D. Turner, private communication). From the stars in common we obtain:  $\Delta V = 0.017 \pm 0.065$ ,  $\Delta(B - V) = 0.014 \pm 0.066$  and  $\Delta(U - B) = 0.034 \pm 0.199$ .

In spite of the significant scatter in the comparison for *U - B*, it can be concluded that the two studies are in nice agreement. The poor match in this color may be ascribed to problems in their *U*-band photometry, as extensively discussed in Sh04. Granted this, as a by-product we confirm that the discrepancies between the photometry Sh04 and that of Wa05 is possibly due to the transformation of the F336 (*U*), F439W (*B*), F555W (*V*) HST photometry to the Johnson-Morgan system.

## 2.4. Astrometry

For two-hundred stars in our photometric catalog there are J2000.0 equatorial coordinates from the Guide Star Catalogue<sup>3</sup>, version 2 (GSC-2.2, 2001). Using the SkyCat tool at ESO, and the IRAF tasks *ccxymatch* and *ccmap*, we first established the transformation between our (*X*, *Y*) pixel coordinates (from ALLSTAR) and the International Celestial Reference Frame (Arias et al. 1995). These transformations turned out to have an *r.m.s.* value of 0.15". Finally, using the IRAF task *cctran*, we computed J2000.0 coordinates for all objects in our catalog.

<sup>3</sup> Space telescope Science Institute, 2001, The Guide Star Catalogue Version 2.2.02.

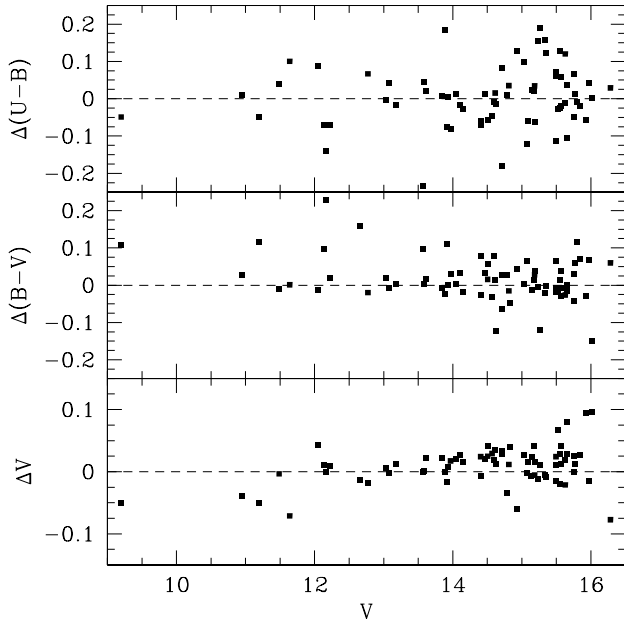


**Fig. 3.** Comparison of our photometry with that of Sh04 for  $V$ ,  $B-V$  and  $U-B$  (in the sense this work minus Sh04), as a function of our  $V$  magnitude.

### 3. The reddening law toward $l=290.63$ and $b=-0.903$

A basic requirement before analyzing our photometric material is to investigate the reddening law in the direction of WR38 and WR38a. Sh04 emphasize that according to their analysis the extinction in this direction follows the normal law, namely that the ratio of total over selective absorption  $\frac{A_V}{E(B-V)}$  is 3.1. This value has already been found to be of general validity towards Carina (Carraro 2002, Tapia et al. 2003). The  $(V-I)$  vs.  $(B-V)$  color-color diagram show in Fig. 4., constructed using our  $UBVI$  photometry, confirms the above statements. Most stars lie close to the reddening-free Schmidt-Kaler (1982) Zero Age Main Sequence (ZAMS) line (dashed line), which runs almost parallel to the reddening vector plotted in the upper-right corner of this figure. This vector has been drawn following the normal extinction ratio (Dean et al. 1978), which suggests that in this specific Galactic direction absorption follows the normal law. In the subsequent discussion we will therefore adopt  $\frac{A_V}{E(B-V)} = 3.1$  and  $\frac{E(U-B)}{E(B-V)} = 0.72$ .

### 4. Stellar populations in the field

In Fig. 5. we present a  $(B-V)$  vs.  $(U-B)$  color-color diagram for those stars in our photometric catalog which have photometric errors lower than 0.05 magnitudes in both  $(B-V)$  and  $(U-B)$ . This figure is similar to Fig. 3 of Sh04, except for the much larger number of stars resulting from our larger area coverage and deeper photometry. The solid line is an empirical reddening-free ZAMS for dwarf stars, from Schmidt-Kaler (1982). In agreement with what was discussed in the previous section, we have adopted a normal reddening law for this region. The corresponding reddening vector has been plotted in the bottom of the figure.

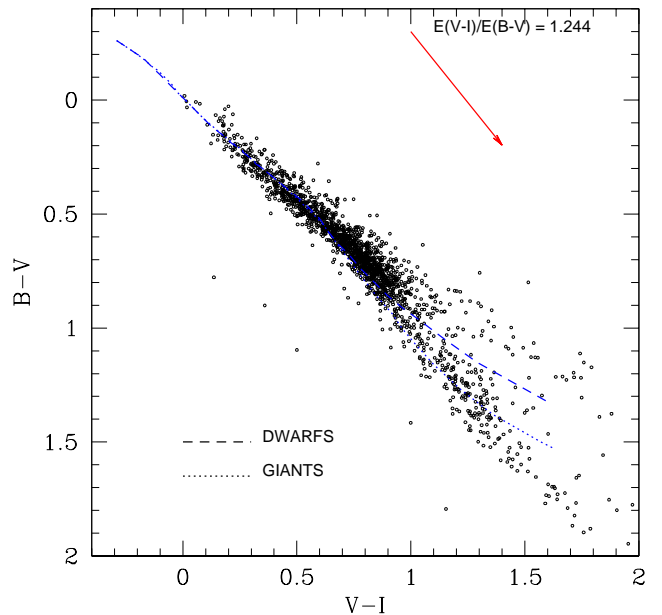


**Fig. 4.**  $(V-I)$  vs.  $(B-V)$  color-color diagram for stars in our field with  $UBVI$  photometry. The reddening vector for the normal extinction law is plotted in the upper-right corner. The dashed and dotted lines represent the reddening-free Schmidt-Kaler (1982) Zero Age Main Sequence relations for dwarf and giant stars, respectively.

Shifting the ZAMS by different amounts in the direction of the reddening vector, we can fit the most obvious stellar sequences, which has led us to identify three distinct stellar populations. This displacement is illustrated by dotted lines (in black) for three spectral type along the reddening direction. This permits to define the spectral type of reddened stars.

In what follows we discuss how we have chosen these amounts and why we claim we are distinguishing three different populations.

The yellow dot-dashed ZAMS has been shifted by  $E(B-V) = 0.25$ , and fits a conspicuous sequence of early type stars. As indicated in the figure, this group is composed by stars of spectral type from as early as O8 up to A0. Beyond A0, the definition of spectral type becomes ambiguous due to the crossing of different reddening ZAMS close to the A0V knee. This low-reddening group of stars clearly suffers from variable extinction, as indicated by the significant spread around the  $E(B-V) = 0.25$  ZAMS. We estimate in fact that the mean reddening for this group is  $0.25 \pm 0.10$ . Sh04 identified this group as stars belonging to the Carina branch of the Carina-Sagittarius spiral arm. We will refer to this group of stars as group A.

The blue short-dashed ZAMS has been shifted by  $E(B-V) = 0.52$ . It passes through a group of young stars, with spectral types ranging from B2 to A0, which exhibit almost no reddening variation. In fact, we estimate that the mean reddening for this group is  $0.52 \pm 0.05$ , namely the scatter around the mean value of 0.52 is small, and compatible with the typical photometric error in the  $(U-B)$  and  $(B-V)$  colors. In Fig. 3 of Sh04 this group is barely visible, and the authors make no comments about it.

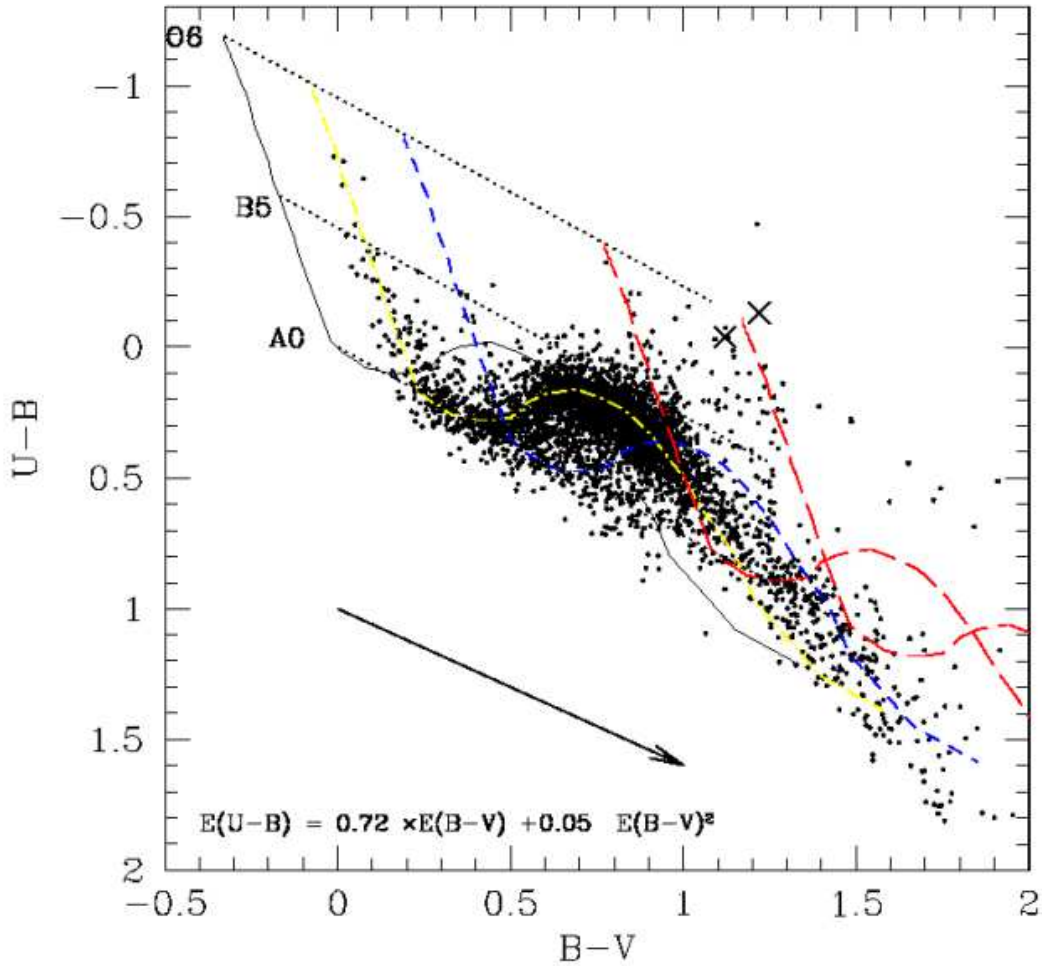


**Fig. 5.**  $(B-V)$  vs.  $(U-B)$  color-color diagram for stars in our photometric catalog with photometric errors lower than 0.05 magnitudes in both  $(B-V)$  and  $(U-B)$ . The reddening vector for the normal extinction law has been plotted in the bottom of the figure. The solid line is an empirical reddening-free ZAMS for dwarf stars, from Schmidt-Kaler (1982). The same ZAMS (dashed lines) has been displaced along the reddening line for three different amounts of reddening, 0.25, 0.52 and 1.45. The approximate location of stars with spectral type O6, B5 and A0 is also indicated. The two crosses are here used to show the position of WR38 and WR38a. See text for more details.

Because of the wider area covered by our study, it could be readily detected in our  $(B-V)$  vs.  $(U-B)$  color-color diagram. We will refer to this group of stars as group **B**.

Similar features (namely secondary sequences in two-color diagrams) have been found in a variety of two-color diagrams of stellar clusters and field stars in the third Galactic Quadrant (see e.g. Carraro et al. 2005). They are thought to be produced by early type stars belonging to distant spiral features in the outer Galactic disk (see also Moitinho et al. 2008).

The two red long-dash ZAMSs have been shifted by  $E(B-V) = 1.10$  and  $E(B-V) = 1.50$ , and identify a group of early-type (from O6 to B5) stars suffering strong reddening with a significant dispersion. Since the region in the color-color diagram between the two red ZAMS is continuously occupied by stars, we propose they basically belong to the same distant population.

We estimate that the mean reddening for this group is  $1.30 \pm 0.20$ . Within this group of stars, Sh04 identify a cluster of young stars surrounding the two WR stars (the two crosses in Fig. 5). We will refer to this group of stars as group **C** or Shorlin 1 (also known as C1104-610a).

As anticipated, the two crosses in Fig. 5 identify the two WR stars; WR38 (WC4) and WR38a (WN5). As exhaustively discussed by Sh04,  $U$ -band photometry of this type of star is difficult, but they do provide corrections to transform their colors to the Johnson-Morgan standard system. Given that our uncorrected colors (see Table 2) are in good agreement with theirs, we adopted their corrections (see the Table 3 in Sh04).

**Table 2.** Photometry of the stars WR38 and WR38a

	V	(B-V)	(U-B)
WR38	14.684	1.216	0.679
WR38a	15.113	1.191	0.077

## 5. Properties of groups A, B and C

To be more quantitative, we first measured the individual reddening of the stars in groups **A**, **B** and **C** using the well known reddening free  $Q$ -parameter (see for instance Johnson 1966), which allows to establish the membership of a certain star to a group on the basis of common reddening (see e.g. Vázquez et al. 1996, Vázquez et al. 2005, and Carraro 2002). Having provided evidences that the reddening law is normal, the  $Q$ -parameter is therefore defined as:

$$Q = (U - B) - 0.72 \times (B - V)$$

The value of  $Q$  is a function of spectral type and absolute magnitude (Schmidt-Kaler 1982).

This technique permits to identify *bona fide* members of similar spectral type as late as A0V. We have identified 146 stars in our sample with a mean  $E(B - V)$  of  $0.25 \pm 0.10$  (group **A**), 96 stars with a mean  $E(B - V)$  of  $0.52 \pm 0.05$  (group **B**), and 212 stars with a mean  $E(B - V)$  of  $1.30 \pm 0.20$  (group **C**).

Then, to obtain an estimate of the mean distance of the three groups, we made use of the variable extinction diagram shown in Fig. 6, where to derive  $(V - M_V)$  we adopt  $M_V$  as a function of spectral type from Schmidt-Kaler 1982. Yellow triangles, blue squares and red circles depict members of groups **A**, **B**, and **C**, respectively. The four lines plotted have been drawn adopting the normal extinction law ( $R_V = 3.1$ ), and correspond to four different absolute distance moduli ( $V_0 - M_V$ ): 10.0 (solid), 12.0 (dotted), 14.0 (short-dashed) and 16.0 (long-dashed). The histograms in the right panel of this figure give the apparent distance moduli distribution, from which we infer the mean distance to the three groups.

One can in fact extrapolate the absolute distance modulus  $(m - M)_{V,0}$  reading the value along the  $Y$ -axis, where the reddening is zero.

In the left panels of figures 7, 8 and 9 we present  $(B - V)$  vs.  $(U - B)$  color-color diagrams enhancing the stars of groups **A** (yellow triangles), **B** (red squares) and **C** (blue circles), respectively. The right panels of these three figures show the distribution on the plane of the sky for the objects in each group. In these latter panels stars have been plotted as circles scaled according to their  $V$  magnitude. The fields shown in these figures are centered at  $RA = 11^h05^m48.5^s$ ,  $DEC = -61^\circ11'5.9''$ . North is up, East to the left as in Fig. 1.

### 5.1. Group A

Inspection of the right panel of Fig. 7 shows that the objects in group **A** are evenly distributed on the sky, with no hints for any particular concentration.

The sequence defined by this group in variable reddening diagram (Fig. 6) has a mean intrinsic distance modulus of

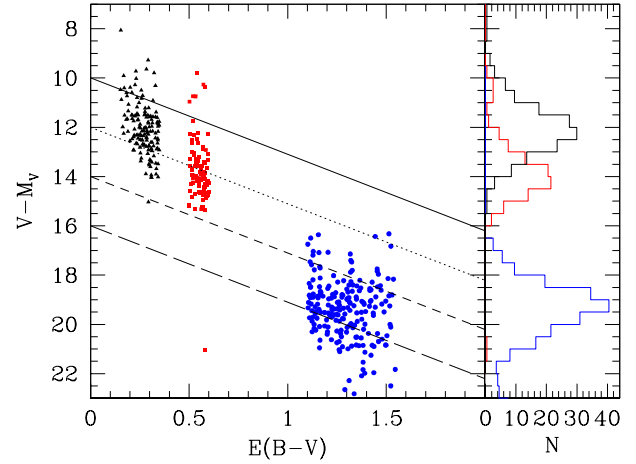


**Fig. 6.** Variable extinction diagram for all early type star for which individual reddening was measured. The four lines plotted have been drawn adopting the normal extinction law ( $R_V = 3.1$ ), and correspond to four different absolute distance moduli ( $V_0 - M_V$ ): 10.0 (solid), 12.0 (dotted), 14.0 (short-dash) and 16.0 (long-dash). The histograms in the right panel of this figure give the apparent distance moduli distribution, from which we infer the mean distance of the three groups.

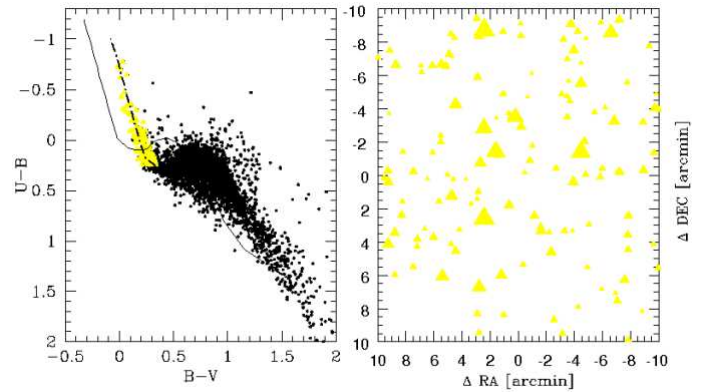


**Fig. 7.** Stars belonging to group **A** (yellow triangles). Left panel (as well as left panel of Fig. 6) illustrates how this group was selected on a reddening basis. See text for details.

12.0 magnitudes, with a large spread. Still, most of the stars lie at a mean distance of  $2.5 \pm 1.5$  kpc. This mean distance is compatible with this group lying in the part of the Carina branch of the Carina-Sagittarius arm closest to the Sun. The observed distance spread is compatible with the typical size of inner Galactic spiral arms (1.5-2.0 kpc, Bronfman et al. 2000).

We therefore conclude that group **A** is composed of young field stars belonging to the Carina-Sagittarius arm, confirming the suggestion by Sh04. We dispute however the possibility that

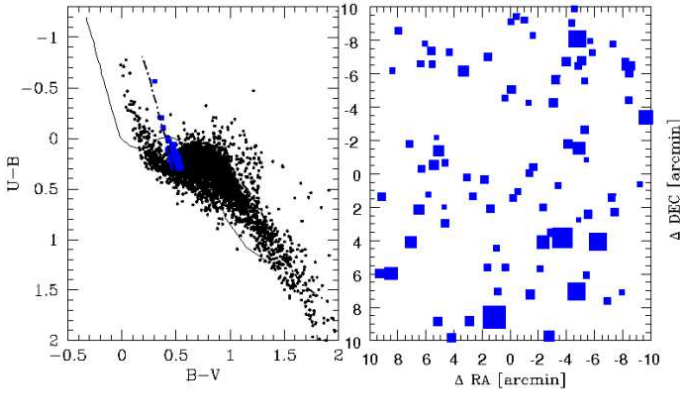


**Fig. 8.** Same as Fig. 6, for stars belonging to group **B** (red squares). See text for details.

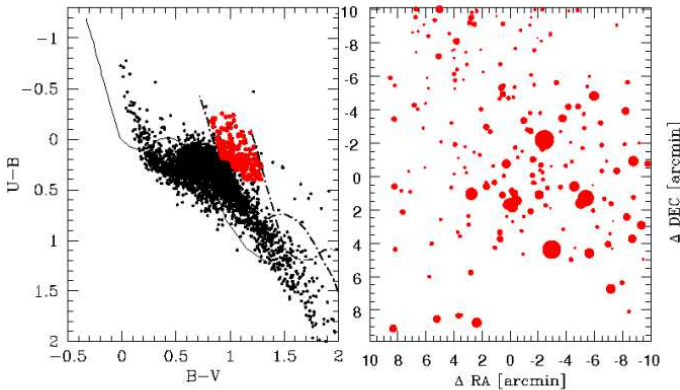


**Fig. 9.** Same as Fig. 6, for stars belonging to group **C** (blue circles). See text for details.

these stars form a star cluster as suggested by Shorlin (1998), and claim that this conclusion was possibly the result of the small FOV covered by the photometry of Shorlin (1998). Our wider coverage clearly shows that we are looking at a population of field stars having the same reddening and age, but located at different distances in the Carina arm.

### 5.2. Group B

As was the case of group **A**, the objects in group **B** are also evenly distributed on the plane of the sky, but they are, on the average, fainter (see right panel of Fig. 8).

In the variable reddening diagram (Fig. 6) they trace a sequence of stars which lie at larger distance than those of group **A**. They have a mean absolute distance modulus of  $14.0$  magnitudes, which implies a bulk distance of  $6.0 \pm 2.0$  kpc. The stars in this group are also young, and, according to modern descriptions of the MW spiral structure (Vallée 2005, Russeil 2003) they are most probably located in the part of the Carina branch more distant from the Sun. In fact, the tangent to the Carina-Sagittarius arm points to  $l \sim 280^\circ$ , in a way that the line of sight to these groups is expected to cross twice the Carina portion of this arm.

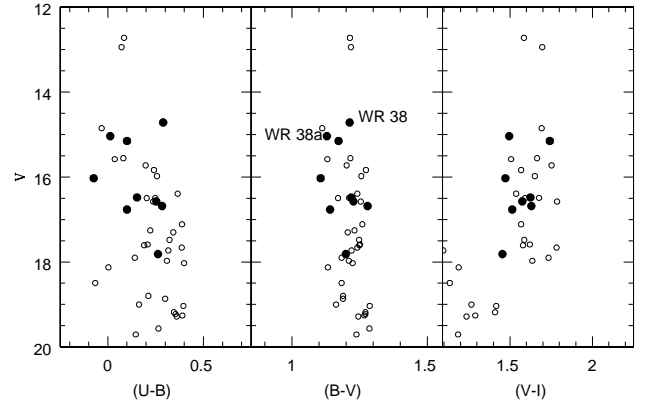


**Fig. 10.** Color-Magnitude Diagrams for stars belonging to group **C**, for different color combinations. Filled symbols indicate stars inside the Shorlin 1 area

This group had not been noticed before, which may be the origin of the different conclusions suggested by Sh04 and Wa05 on the location, and distance, of the putative star cluster associated to WR38 and WR38a (see discussion below).

### 5.3. Group C

This is the most interesting group of faint young stars with common reddening. Our mean  $E(B - V)$  value ( $1.30 \pm 0.20$ ) is smaller than the value found by Sh04, but still marginally compatible within the errors declared. The 212 stars extracted within this reddening range have a broad distance distribution (see Fig. 6), are faint, and fairly evenly distributed across the field of view (see Fig. 9). Careful inspection of Fig. 9 indicates the existence of a concentration of stars close to the center of the field. This concentration corresponds to Shorlin 1 (C1104-610a, Sh04).

The point now is whether this is really a cluster or just a chance concentration of bright stars- and where it lies exactly. As Sh04 argue, the reality of the cluster can be assessed only with much deeper photometry. To address these two issues we will make use of the variable reddening diagram (Fig. 6) and of the CMDs presented in Fig 10 and Fig. 11, constructed with the objects belonging to group **C** having the largest reddening ( $E(B-V) > 1.45$ ), as Shorlin 1 (see Sh04). Filled symbols in Figs. 10 and 11 indicate stars within a  $0.6'$  wide circle centered on Shorlin 1 (nominal center  $RA = 11^h05^m46.52^{sec}$ ;  $DEC = -61^\circ13'49.1''$ ), which is the zone where the cluster seems to be located.

Given that these common reddening stars of group **C** distribute evenly in the field (see Fig. 9), we can compare the position (in a CMD) of objects in the general field with that of objects in the Shorlin 1 region. As shown by the CMDs presented in Fig. 10, general field stars (open symbols) occupy the same region as Shorlin 1 stars (filled symbols). This suggests that they share the same distance range and age, and therefore conform a common properties, evenly distributed, population.

The same conclusion can be drawn from the reddening-free CMDs presented in Fig. 11. In these plots the stars within the putative cluster area and those in the general field define the same sequence. The  $V_o$  vs.  $(B - V)_o$  CMD presented in the

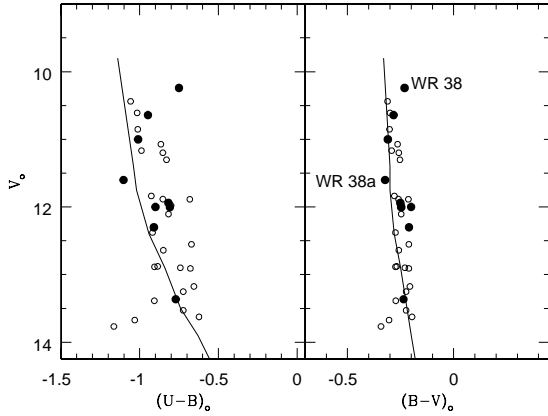


**Fig. 11.** Reddening free Color-Magnitude Diagram for stars belonging to group **C**, for different color combinations. Filled symbols indicate stars inside Shorlin 1 area. In this figure only stars having  $E(B-V)$  larger than 1.45 are plotted. See text for more details.

right panel of Fig. 11 has been plotted in the same scale as Fig. 5 of Sho04. Note that, in spite of our photometry being six magnitudes deeper in  $V$ , we detect only one fainter object in the cluster area. We can be confident therefore that there are no fainter stars associated to the cluster.

The ZAMS superposed in the both panels of Fig. 11 is for  $(m-M)_{V,o} = 15.5$ , which suggests that the distance of group **C** is about  $12.7 \pm 3.0$  kpc. Both Shorlin 1 members and field stars exhibit however a significant distance spread (see Fig. 6)

For the reasons summarized below, we conclude that there is no clear evidence of a star cluster at the location of WR38/WR38a.

- a cluster hosting two WR stars would have to be a relatively massive one, with numerous stars of spectral type later than B; on the contrary to what we see,
- we do not see any special concentration of stars at the putative cluster location (see Fig. 1),
- the sequence defined by Shorlin 1 in the CMDs is also occupied by field stars which have the same reddening, and are evenly distributed in the field (see Figs. 9, 10 and 11),
- the stars defining the cluster (the 8 stars discovered by Sh04, plus one fainter object from this work) exhibit a significant distance spread (see Fig. 6), incompatible with a physical, although loose, star cluster.

To summarize our findings, we report in Table 3 the main properties of the three groups. As for the age we only provide an upper limit, since the populations under investigations are surely young, and a precise age estimate - by the way quite difficult - is beyond the scope of this work.

## 6. Conclusions

The large angular coverage, and depth, of our  $UBVI$  photometry of the region around the WR38/WR38a has allowed us to clarify the stellar populations towards Galactic longitude  $\approx 290^\circ$ , in the fourth Galactic quadrant.

**Table 3.** Properties of the three distinct groups we detected in the field toward WR 38 and WR 38a.

Group	$E(B-V)$	$d_\odot$	age	Note
A	$0.25 \pm 0.10$	$2.5 \pm 1.5$	$< 100$ Myr	Carina
B	$0.52 \pm 0.05$	$6.0 \pm 2.0$	$< 100$ Myr	Carina
C	$1.30 \pm 0.20$	$12.7 \pm 3.0$	$< 100$ Myr	Perseus

Our results can be visualized with the aid of Fig. 12, where the spiral structure of the Galaxy (Vallée 2005) is presented in the  $X - Y$  plane, where  $X$  points in the direction of Galactic rotation and  $Y$  points towards the anti-center. The Carina and Perseus arms are indicated with the symbols *I* and *II*, respectively. The Galactic center and the position of the Sun are also indicated, at  $(0.0, 0.0)$  and  $(0.0, 8.5)$ , respectively. The position, pitch angle, and extension of the arms are clearly model dependent; to a lesser extent for the Carina arm (which is well known) and significantly more for the less-known Perseus arm (both HI observations (Levine et al. 2006) and HII observations (Rusell 2003) coincide however on the approximate location and extent of the Perseus arm). Beyond  $\sim 9$  kpc from the Sun, it is not expected to find spiral features related to the Carina arm (Georgelin et al. 2000); more distant structures can be associated with the Perseus arm. According to Levine et al. (2006, their Fig. 4) at  $l=290^\circ$  the Perseus arm is located in the range  $-18.0 \leq X \leq -13.0$  and  $0.0 \leq Y \leq 2.0$  Kpc, respectively, in nice agreement with Vallée model.

With a dashed arrow we indicate the line-of-sight in the direction of our field, and with thick segments the distance range we derived for the three groups (**A**, **B** and **C**) we identified in this Galactic direction (see also Table 3). Fig. 12 shows that the groups detected remarkably fit the position of the Carina and Perseus arm. This confirms Sh04's suggestion that the most distant group (**C**) is most probably associated with the extension of the Perseus arm in the fourth Galactic quadrant, and constitutes the first optical detection of this arm. However, on the contrary to Sh04, here we propose that this extreme group is not a star cluster, but simply a group of young stars uniformly distributed within the Perseus arm.

The direction we are investigating is about  $\sim 1^\circ$  below the Galactic plane. At distances of 2.5, 6.0 and 12.7 kpc this implies heights below the Galactic plane of about 50, 100, and 210 pc, respectively. These are sizeable values, and reflect the trend of the Galactic warp in this zone of the disk (Momany et al. 2006).

We finally wish to discuss our photometric database in the framework of a possible detection of the Argus over-density discussed in Rocha-Pinto et al. (2006), or the Monoceros Ring, which Shorlin 1 was suggested to be associated with (Frinchaboy et al. 2004). With this aim, in Fig. 13 we present  $V$  vs.  $(B - V)$  CMD for all the stars having BV photometry.

The distribution of stars in this diagram is relatively easy to describe. Apart from the prominent blue sequence of young stars brighter than  $V \approx 14.0$ , which are the objects of **A**, we can distinguish two other remarkable features. The first is a thick Main Sequence (MS) downward of  $V \approx 14.0$ , widened by photometric errors and binaries, but mostly reflecting the fact we are sampling objects at very different distances, and with different reddening, in the Galactic disk. Along this thick MS

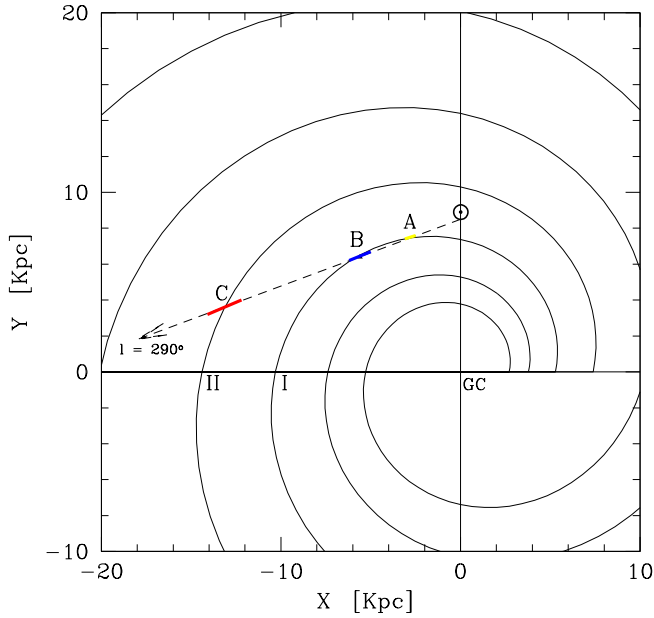


**Fig. 12.** Schematic view of the spiral structure of the Galaxy (Vallée 2005).  $X$  points in the direction of Galactic rotation, and  $Y$  points towards the anti-center. The position of the Sun (0.0,8.5) and of the Galactic center (0.0,0.0) are indicated. The symbols I and II indicate the Carina and Perseus spiral arms, respectively. Thick segments illustrate the location of the three groups (A, B and C) discussed in the text. See text for details

we do not find any evidence of a blue Turn Off Point, typical of the metal poor, intermediate age, population of the Monoceros Ring (Conn et al 2007).

Therefore we conclude that no indication of the presence of the Monoceros Ring or the Argus system is detected in our field.

The second is a Red Giant Branch, significantly widened and somewhat bent by variable reddening, composed of giant stars at different distances. The relatively high number of giants can be easily accounted for, because we are sampling a field located  $1^\circ$  below the Galactic plane.

Our results confirm the effectiveness of multicolor optical photometry in the study of the structure of the MW disk. More fields need to be observed to better constrain the spiral structure in the fourth Galactic quadrant, in particular the shape and extent of the Perseus arm, and, possibly, detect the more distant Norma-Cygnus arm.

At odds with radio observations, which has to rely on the poorly known Galactic rotation curve, optical observation, especially in low absorption directions, can better constraint the distance to spiral features.

*Acknowledgements.* Tomer Tal and Jeff Kenney are deeply thanked for securing part of the observations used in this paper. GC acknowledges R.A.Vázquez for very fruitful discussions. EC acknowledges the Chilean Centro de Astrofísica FONDAP (No. 15010003).

## References

Arias, E. F., Charlot, P., Feissel, M., & Lestrade, J.-F. 1995, *A&A*, 303, 604  
 Benjamin, R.A., 2008, in *Massive Star Formation: Observations Confront Theory*, ASP Conference Series, Vol. 387, p. 375  
 Bronfman, L., Casassus, S., May, J., Nyman, L.-Å. 2000, *A&A* 358, 521

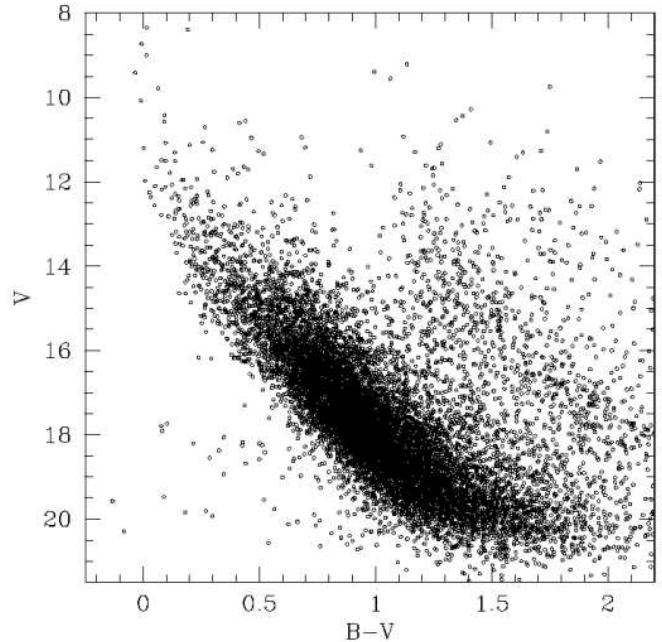


**Fig. 13.** CMD of all stars with BV photometry in the field under study

Carraro, G., 2002, *MNRAS* 331, 785  
 Carraro, G., Vázquez, R.A., Moitinho, A., Baume, G., 2005 *ApJ* 630, L153  
 Conn, B.C., Lane, R.R., Lewis, G.F. et al., 2007, *MNRAS* 376, 939  
 Dean, J.F., Warren, P.R., Cousins, A.W.J., 1978, *MNRAS* 183, 569  
 Frinchaboy, P.M., Majewski, S.R., Crane, J.D., et al. 2004, *ApJ* 603, L21  
 Georgelin, Y.M., Russeil, D., Amram, P., Georgelin, Y.P., Marcelin, M., Parker, Q.A., Viale, A., 2000, *A&A* 357, 308  
 Johnson, H.L., 1966, *ARA&A* 4, 193  
 Landolt, A.U., 1992, *AJ*, 104, 372  
 Luna, A., Bronfman, L., Carrasco, L., Maj, J., 2006, *ApJ* 641, 938  
 Levine, E.S., Bliz, L., Heiles, C., 2006, *Science* 312, 1773  
 Moitinho, A., Vázquez, R.A., Carraro, G., Baume, G., Giorgi, E.E., & Lyra, W. 2006, *MNRAS*, 368, L77  
 Moitinho, A., Vázquez, R.A., Carraro, G., 2008, *A&A*, to be submitted  
 Martin, N.F., Ibata, R.A., Bellazzini, M., Irwin, M.J., Lewis, G.F., Dehnen, W., 2004, *MNRAS*, 348, 12  
 Momany, Y., Zaggia, S., Gilmore, G., Piotto, G., Carraro, G., Bedin, L., de Angeli, F., 2006, *A&A* 451, 515  
 Patat, F., Carraro, G., 2001, *MNRAS* 325, 1591  
 Rocha-Pinto, H.J., Majewski, S.R., Skrutskie, M.F., Patterson, R.J., Nakanishi, H., Muñoz, R.R., Sofue, Y., 2006, *ApJ* 640, L147  
 Russeil, D., 2003, *A&A* 397, 133  
 Schmidt-Kaler, Th., 1982, Landolt-Börnstein, Numerical data and Functional Relationships in Science and Technology, New Series, Group VI, Vol. 2(b), K. Schaifers and H.H. Voigt Eds., Springer Verlag, Berlin, p.14  
 Shorlin, S.L., 1998, M.Sc. thesis, Saint Mary's University  
 Shorlin, S.L., Turner, D.G., Pedreros, M., 2004, *PASP* 116, 170 (Sh04)  
 Stetson, P.B., 1987, *PASP*, 99, 191  
 Tapia, M., Roth, M., Vázquez, R.A., Feinstein, A., 2003, *MNRAS* 339, 44  
 Vallée, J.P., 2005, *AJ* 130, 569  
 Vázquez, R.A., Baume, G.L., Feinstein, C., Prado, P., 1996, *A&A* 116, 75  
 Vázquez, R.A., Baume, G.L., Feinstein, C., Nuñez, J.A., Vergne, M.M., 2005, *A&A* 430, 471  
 Vázquez, R.A., May, J., Carraro, G., Bronfman, L., Moitinho, A., Baume, G., 2008, *ApJ* 672, 930  
 Wallace, D.J., Gies, D.R., Moffat, A.F.J., Shara, M.M., Niemela, V., 2005, *AJ* 130, 126 (Wa05)  
 Yanny, B., Newberg, H.J., Grebel, E.K., Kent, S. et al., 2003 *ApJ* 588, 824